BIOCHEMISTRY
including biophysical chemistry & molecular biology

ARTICLE

pubs.acs.org/biochemistry

Heterogeneous Amylin Fibril Growth Mechanisms Imaged by Total Internal Reflection Fluorescence Microscopy

Sharadrao M. Patil, Andrew Mehta, Suman Jha, and Andrei T. Alexandrescu*

Department of Molecular and Cell Biology, University of Connecticut, Storrs, Connecticut 06269-3125, United States

Supporting Information

ABSTRACT: Total internal reflection fluorescence microscopy has been used to visualize the fibrillization of amylin, a hormone which in aggregated forms plays a role in type 2 diabetes pathology. Data were obtained at acidic pH where fibrillization is hindered by the charging of histidine 18 and at slightly basic pH where the loss of charge on the histidine promotes aggregation. The experiments show three types of aggregate growth processes. In the earliest steps globular seeds are formed with some expanding radially during the course of the reaction. The dimensions of the globular seeds as well as their staining with the amyloid-specific dye thioflavin T indicate that they are plaques of short fibrils. The next species observed are fibrils that invariably grow from large globular seeds or smaller punctate granules. Fibril elongation appears to be unidirectional, although in some cases multiple fibrils radiate from a single seed or granule. After fibrils are formed, some show an increase in fluorescence intensity that we attribute to the growth of new fibrils alongside those previously formed. All three aggregation processes are suggestive of secondary (heterogeneous) nucleation mechanisms in which nucleation occurs on preformed fibrils. Consistently, electron micrographs show changes in fibril morphology well after fibrils are first formed, and the growth processes observed by fluorescence microscopy occur after the corresponding solution reactions have reached an initial apparent plateau. Taken together, the results highlight the importance of secondary nucleation in the fibrillization of amylin, as this could provide a pathway to continue fibril growth once an initial population of fibrils is established.

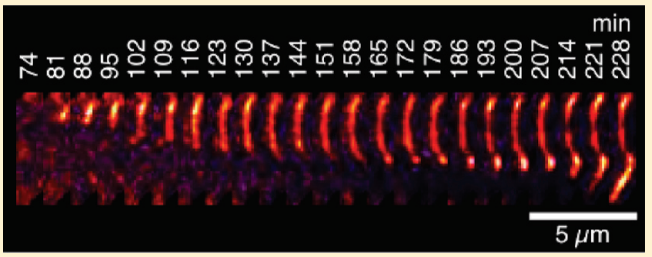

Amylin, also known as IAPP, is a 37-residue (4 kDa) endocrine hormone thought to play key roles in the pathology of type 2 diabetes.[1−5] The normal physiological functions of amylin include regulating blood glucose in concert with insulin, inhibiting glucagon secretion, slowing down the emptying of the stomach, and inducing a feeling of satiety.[3,5] Amylin levels increase in a number of diseases including obesity, syndrome X, pancreatic cancer, and renal failure.[3] In patients with type 2 diabetes amylin levels initially increase and then fall as the disease advances to the point where the pancreatic β-cells that make amylin and insulin are destroyed.[3] Amylin is the main component of amyloid deposits found in the interstitial fluid between pancreatic islet cells of patients with type 2 diabetes.[1−3] The amyloid causes changes in the morphology of pancreatic β-cells,[3] and aggregates of amylin are toxic when added to cultures of β-cells.[6,7] In several transgenic mouse and rat models, expression of human amylin has been found to correlate with β-cell apoptosis and diabetes-like symptoms,[8] although considerable controversy surrounds the issue of whether the fibrils themselves or smaller oligomeric precursors are responsible for deleterious effects.[9−12] Genetic evidence that links amylin to type 2 diabetes comes from the familial S20G mutation which leads to early onset of the disease[13] and produces an amylin variant that aggregates more readily.[14] Type 2 diabetes affects about 200 million people worldwide, and its incidence is expected to reach 300 million by 2025.[15,16] Understanding the mechanisms responsible for amylin aggregation and toxicity will become increasingly important in formulating new approaches to disease treatment.

In the present study we used TIRFM in conjunction with the amyloid specific dye ThT to follow the growth processes of individual amylin aggregates. At the interface between a medium with a large refractive index (glass slide) and a medium with a small refractive index (aqueous solution), laser excitation can be used to induce a thin 100−200 nm electromagnetic field called an "evanescent wave" in the medium with the smaller refractive index.[17−19] This narrow illumination field can be used for TIRFM imaging of objects lying along the plane of the coverslip.[17] Compared to conventional fluorescence microscopy, background fluorescence from fluorophores in bulk solution decreases exponentially with distance from the slide−solution interface in TIRFM.[19] While TIRFM has the same resolution as light microscopy, the exquisite sensitivity of the technique makes it possible to detect single molecules.

The application of TIRFM to the study of individual amyloid fibrils was pioneered by the Goto lab, who used the technique to study growth process of amyloid fibrils formed by the Alzheimer's

Received: November 30, 2010
Revised: March 10, 2011
Published: March 10, 2011

Aβ(1−40) peptide, glucagon, and β2-microglobulin.[17,20−23] The amyloid-specific dye ThT was used to image the fibrils. Binding of ThT to amyloid fibrils causes marked changes in the fluorescence spectrum of the dye. These include red shifts in the excitation maximum from 385 to 450 nm and in the emission maximum from 445 to 482 nm and a large increase in quantum yield when the dye is bound to the amyloid cross-β structure.[24] These properties make ThT ideal for imaging amyloid fibrils by TIRFM, since fluorescence from the free dye in solution is minimal and the dye is specific to amyloid fibrils.[17] Conversely, aggregates that lack the specific cross-β sheet structure of amyloid fibrils will be invisible to TIRFM imaging using ThT. Alternatively, fluorescent dyes can be covalently attached to amyloidogenic proteins to image their fibrillization.[25−27] Pioneering studies of amyloid fibrils by TIRFM provided important information on the kinetics of individual fibril growth starting from seeded reactions and on the unidirectional polarity of fibril elongation[21,22,25−27] predicted by fibril structure composed primarily of parallel β-sheets.

Here, we use TIRFM to image amylin aggregation. Previous TIRFM studies looked at fibril elongation starting from seeded solutions; that is, mature fibrils were fragmented by sonication to provide nucleation sites for fibril growth.[20−22] Because amylin fibrillization is fast and because we wanted to investigate seed formation, the reactions in the present work were not seeded. Because we were interested in the effects of charge on amylin fibrillization, we obtained TIRFM data under acidic conditions close to those the hormone experiences when it is stored in β-cell secretory granules, and near the neutral pH conditions amylin is exposed to when it is released into the extracellular matrix.[28] Data on the growth of individual aggregates on the surface of a slide monitored by TIRFM were compared to snapshots sampling the population of aggregates that develop in solution using the higher resolution afforded by EM. Kinetics of individual fibrillar aggregates measured by TIRFM were compared with fibrillization kinetics in solution measured by fluorescence spectroscopy. Our results indicate that amylin fibrillization proceeds through multiple mechanisms involving a mixture of fibril species and emphasize the importance of secondary nucleation[20,29−31] in amylin fibrillization.

EXPERIMENTAL PROCEDURES

Sample Preparation. Human amylin containing an amidated C-terminus and a Cys2−Cys7 disulfide bond was purchased from Anaspec (Cat. No. 60254-05; San Jose, CA). The peptide, which was >95% pure, was supplied as a dry powder in 0.1 mg amounts sealed in glass vials. Because the peptide is poorly soluble in water, samples were dissolved in 10% acetonitrile (ACN) according to the manufacturer's suggestion. A 20 mM sodium phosphate buffer was used for studies at pH 8 while a 60 mM sodium citrate buffer was used for experiments at pH 4. Additional experiments were done in which the peptide was initially dissolved in 100% DMSO before adjusting the samples to a final concentration of 4% (v/v) DMSO in aqueous buffers. Amylin solutions were used immediately or stored at −80 °C. Unless otherwise specified, the final amylin concentrations in all samples was 100 μM. This peptide concentration was chosen because it gave the best results for TIRFM experiments in terms of the number of fibrils formed and the speed of the fibrillization reactions. The samples additionally contained the metal chelator EDTA at a 0.5 mM concentration and the bacteriostatic compound sodium azide at a 0.05 mM concentration. Before use in fibrillization reactions, the solutions were sonicated continuously for 5 min in an ice bath at a power of 75% using a Fisher Scientific Sonic Dismembrator Model 500.

TIRFM Experiments. Fibrils were imaged using the fluorescent dye ThT (Ultrapure, Anaspec; San Jose, CA) which was included in the samples at a concentration of 5 μM. Samples of ∼30 μL were inserted in the space between a glass slide (Fisher Cat. No. 12-544-1) and a clean coverslip (Fisher Cat. No. 12-542-C; Pittsburgh, PA), affixed on two edges with double-sided tape. The assembly was sealed with Dow Corning high-vacuum grease and placed on the microscope with the coverslip facing the objective. Glass coverslips were cleaned by soaking for 1 h in 2:1 (v/v) HNO_3:HCl, washing with water, and rinsing three times with deionized water. Coverslips were stored in 70% ethanol and dried before use. Glass slides were prepared in the same way except they were cleaned with a 1% (w/v) Alconox solution.

Fibril growth was imaged using a TIRFM system integrated into an Andor Revolution XD Spinning Disk Confocal instrument with a Nikon TiE inverted microscope. ThT excitation was achieved at 405 nm, using the available laser line on our instrument closest to the excitation maximum of 450 nm for amyloid-bound ThT.[24] Excitation profiles for amyloid-bound ThT recorded on a standard fluorescence spectrophotometer were used to establish that excitation at 405 nm leads to an ∼50% loss in fluorescence intensity compared to excitation at 450 nm. Although this results in a loss of sensitivity, ThT excitation at 405 nm can still be used to visualize fibrils. To selectively monitor fluorescence from amyloid-bound ThT which has an emission maximum of 482 nm,[24] we used a 483 ± 16 nm bandpass filter from Semrock (Rochester, NY). Images were recorded with an Andor 897 iXon EMCCD camera using an oil immersion TIRF lens (1.49 NA, 100×, Nikon). Samples were maintained at a temperature of 24 ± 1 °C during the experiments. We did additional experiments on a Leica TCS SP2 laser confocal scanning microscope to verify that the seedlike aggregates imaged by TIRFM were detected due to ThT fluorescence. For these experiments we excited the sample at a fixed wavelength of 458 nm and scanned through the emission spectrum which had a maximum at 483 nm, consistent with the fluorescence maximum of amyloid-bound ThT.[24] Image analysis, including calculations of fibril lengths and seed diameters, was performed with ImageJ software from the NIH.[32] Briefly, the "set scale" utility of ImageJ was used for calibration according to the resolution of our camera which was 133 nm/pixel. The line utility was then used to measure the length or diameters of objects. Curved fibrils were approximated by line segments, and their lengths were calculated from the sum of the segments. To characterize kinetics, length were measured every 2 h of the 48 h experiment at pH 4 and every 1 h of the 23 h experiment at pH 8. When measuring kinetics, we excluded any species that appeared between consecutive TIRFM images collected 5 or 15 min apart and then maintained a constant size, since these are likely to represent aggregates that have precipitated from solution onto the coverslip.[21,22]

EM Experiments. Samples containing 100 μM amylin at pH 8 or pH 4 were incubated at 25 °C, and aliquots of the reaction were removed for imaging after 0.5, 5, 10, 20, and 170 h (1 week). Aliquots were immediately transferred to 400-mesh carbon-coated Maxtaform Cu/Rh grids (Ted Pella Inc., Redding, CA) and stained with a 1% (w/v) solution of uranyl acetate. EM images were recorded using an AMT XR-40 (2048 × 2048 pixel) camera that was side-mounted on a Tecnai BioTWIN G^2 Sprit

transmission electron microscope. At least five images were obtained for each sample and time point, and the most representative images were analyzed.

Fibrillization Kinetics in Solution. The time course of fibrillization in solution was monitored in duplicate using 200 μL samples of amylin, contained in white polystyrene clear-bottom 96-well plates (Corning Inc., Corning, NY). Plates were covered with a clear polyester sealing tape (Fisher Scientific, Agawam, MA) to prevent evaporation. Samples had 100 μM amylin concentrations for consistency with the TIRF experiments and 10 μM ThT (Sigma; St. Louis, MO). To look at the effects of predissolving amylin in different organic solvents, we compared amylin dissolved in pure ACN and brought up in buffer to a final concentration of 10% (v/v) ACN to amylin dissolved in pure DMSO and brought up to a concentration of 4% (v/v) DMSO. All experiments were done without agitation, at a temperature of 25 °C. ThT fluorescence was recorded at 1 min intervals for 30 h using excitation at 440 nm and emission at 490 nm on a Fluoroskan Ascent 2.5 fluorescence plate reader.

RESULTS

TIRF Microscopy of Amylin Fibrillization at pH 4 and 8. Fibrillization of amylin is enhanced at pH 8 compared to pH 4 due to the loss of the positive charge on His18, which lessens electrostatic repulsion between the amylin monomers packed in fibrils [ref 28 and Sheftic, S., Jha, S., and Alexandrescu, A. T., in preparation]. These effects are physiologically relevant since amylin is stored at pH 5.5 in the secretory granules of pancreatic β-cells but is exposed to pH 7.4 when it is released into the extracellular matrix.[28] To look at the effect of pH on fibrillization, we obtained TIRFM data at pH 4 and 8, where His18 in amylin fibrils is fully charged and fully uncharged, respectively [Sheftic, S., Jha, S., and Alexandrescu, A. T., in preparation]. Movies of the reactions at the two pH values are included in the Supporting Information.

Figure 1 shows 42 × 42 μm sections of the 68 × 68 μm TIRFM images collected. The earliest images obtained after 45 min (Figure 1A,C) are compared with images at the end of the reactions: 48 h at pH 4 (Figure 1B) and 23 h at pH 8 (Figure 1D). The first images at both pH values show mostly round "seeds" (Figure 1A,C), even though no attempt was made to seed the reaction by fragmenting preformed fibrils.[17,21,22] Because amylin fibrillization is fast, some seeds and a few fibrils already formed during the 45 min lag time of the experiment between dissolution of the peptide and TIRFM imaging. In addition to seeds, we observed smaller punctate "granules". We use the terms seed to describe aggregates with a round, nonfibrillar morphology for consistency with previous studies[17,21,22] and because the growth of the fibrils we see by TIRFM invariably starts from these aggregates. As we show below, the dimensions of the seeds together with their binding of the amyloid-specific dye ThT (which is a prerequisite for TIRFM observation) indicate they correspond to plaques of short fibrils rather than the oligomeric nuclei that initiate fibril growth through primary nucleation mechanisms. The number of seeds initially observed at pH 8 (Figure 1C) was larger than at pH 4 (Figure 1A). As the reaction progressed, more fibrils formed at pH 8 (Figure 1D) than at pH 4 (Figure 1B) and the fibrils at pH 8 were more clustered (Figure 1D). The smallest objects we could identify were about 0.2 μm (200 nm) as the resolution of our camera is 133 nm/pixel. Although we counted objects with sizes between 0.2 and 0.5 μm as small seeds, we caution that we cannot easily distinguish between a round seed and an elongated fibril morphology for objects smaller than about 0.5 μm.

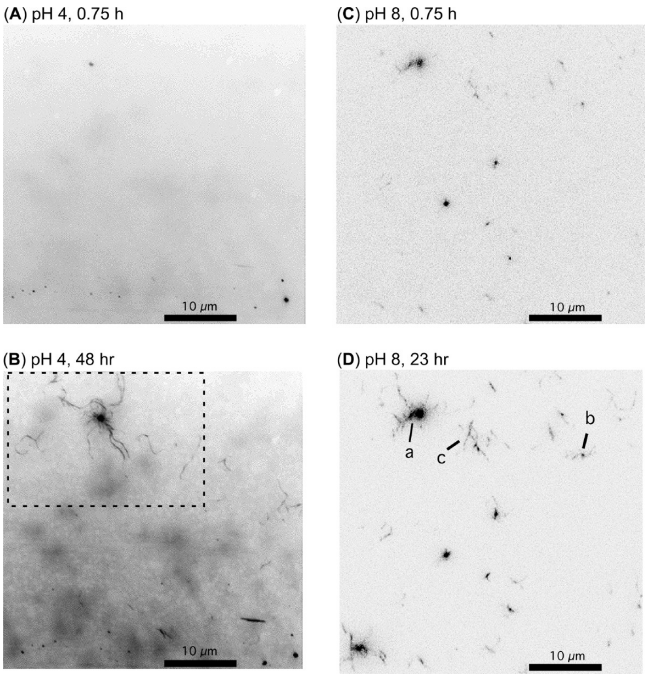

Figure 1. TIRFM images of human amylin at pH 4 (A, B) or pH 8 (C, D) showing the initial (A, C) and final stages of the reactions (B, D). Images were color inverted so that white corresponds to nonfluorescent material and black to fibril-induced ThT fluorescence. The dashed box in (B) corresponds to the area shown in Figure 4. In panel D, *a* is an example of a large seed, *b* is an example of a small seed (granule) with at least two faint fibrils emanating from it, and *c* is an example of a fibril.

Figure 2 compares the distributions of seed and fibril lengths at the end of the reactions, when no further changes were seen in the TIRFM images. Qualitatively, we have seen between a 2- and 5-fold increase in the numbers of seeds and fibrils at pH 8 compared to pH 4 in multiple TIRFM experiments. A quantitative assessment is not possible because we are not observing a macroscopic average. The number of individual aggregates varies between experiments or even when different sections of a slide are compared. The distributions of seeds and fibril lengths, however, show similar patterns in multiple experiments. At both pH values there were about twice as many fibrils as seeds at the end of the reaction, while seeds were the dominant species at the start of the reaction. The average fibril lengths when the reactions reached completion were ~2 μm at both pH values although a small number of fibrils as long as 5−7 μm were observed (Figure 2). Seed diameters were on average about 50% larger at pH 8 (0.56 μm, 60 samples) compared to pH 4 (0.34 μm, 29 samples) while fibril lengths were the same. The distributions of seed sizes fell of more rapidly than fibrils (Figure 2), suggesting that large seeds are unstable or disfavored.

Seeds Observed by TIRFM Correspond to Plaques of Short Fibrils. Figure 3 shows a small seedlike object with a 0.15 μm diameter imaged by EM that is comparable to the 0.35 μm diameter of seed *b* in the TIRF image of Figure 1D. The subsequent EM images in Figure 3 shown progressively higher magnifications of the areas indicated by the rectangles. As the resolution of the EM images increases, the globular seed can be

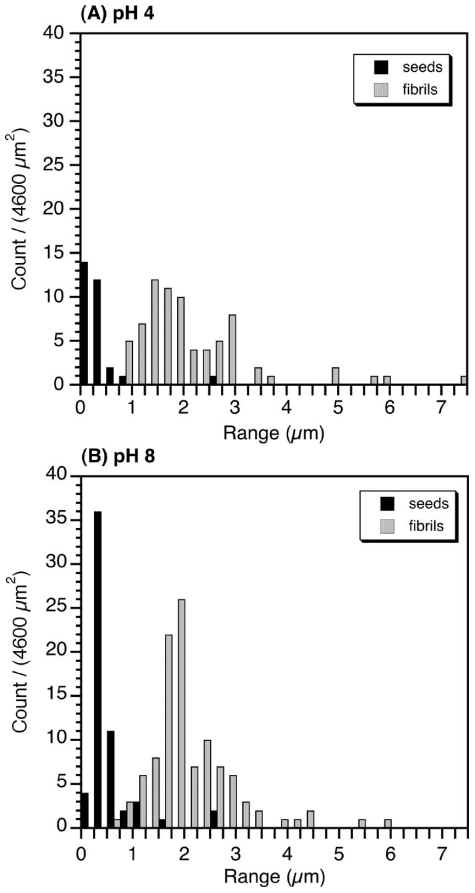

Figure 2. Distributions of seeds and fibrils at the last time points of the TIRF experiments (A) at pH 4, after 48 h of incubation and (B) at pH 8, after 23 h of incubation. By these times fibril growth processes had subsided for each of the samples.

seen to be composed of a cluster of small wormlike fibrils. A similar series of images at different magnifications are provided in the Supporting Information for a larger seed that at high resolution can be seen to be composed of a dense meshwork of fibrils.

AFM studies reported that in the initial stages of amylin fibrillization globular oligomers are formed with an average length of 23 nm. The oligomers grew in height from 2 to 6 nm before elongating into fibrils.[33] The sizes of the oligomers observed by AFM are some 10−100 times smaller than the smallest 0.2 μm sized aggregates discernible by TIRFM. In EM images of amylin fibrillization reactions we see some fibrils as short as 10−20 nm, but these have an elongated rather than a globular morphology. For objects shorter than about 10 nm it would be difficult to distinguish between a fibrillar and globular morphology. Globular aggregates that could correspond to the types of oligomeric intermediates seen by AFM were not seen by EM under the conditions of our study.

The oligomeric species observed by AFM elongated into fibrils in about 30−60 min.[33] This time scale is on the order of our 20−45 min dead time for preparation of samples for EM and TIRFM experiments. Moreover, the AFM studies were done with 10 μM amylin concentrations,[33] which should result in slower fibrillization kinetics than at the 100 μM amylin concentrations used for this work. Some of the seeds observed by TIRFM grow over periods of 10−20 h, a rate much slower than the lifetime of the globular oligomers observed by AFM.[33] Moreover, nearly all of the seeds observed by TIRFM persisted at the ends of the 24 h (pH 8) or 48 h (pH 4) experiments, whereas for a primary nucleation mechanism, the population of oligomeric species should decrease at the expense of fibrils during the course of the reaction.[33] Finally, the detection of species by TIRFM through ThT fluorescence requires that amylin is assembled in a cross-β conformation. The specific changes in ThT fluorescence when the dye binds fibrils generally do not occur when the dye binds oligomers.[34] We therefore conclude that the seeds observed by TIRFM are plaques of short fibrils. The seeds observed by TIRFM can clearly act as nucleation sites for fibril growth, since all of the fibrils we observed start from small seeds or granules. The growth processes, however, are more consistent with a secondary or heterogeneous nucleation mechanism than with the primary or homogeneous nucleation events that lead to the formation of the initial fibrils following the lag phase of fibrillization.

TIRF Microscopy Reveals Three Distinct Mechanisms of Aggregation. Figure 4 shows snapshots of an amylin aggregation reaction at pH 4. The data are illustrated for pH 4 because fibrillization kinetics are slower and there are fewer fibrils under these conditions, making it easier to show key steps in the reaction. Aggregation mechanisms were similar at pH 8, except where noted. The principal differences were that at pH 8 more fibrils formed and these were more clustered.

The time course of aggregation in Figure 4 suggests three distinct aggregation mechanisms: seed growth, fibril elongation, and fibril thickening. The three types of aggregation mechanisms are discussed in detail below.

Radial Seed Growth. The first species observed in experiments at both pH 4 and 8 are seeds illustrated by aggregates *a* and *b* in Figure 4. After fibrils started to grow, few if any new seeds were observed. Some seeds such as *a* grew in intensity and expand radially with time, while the majority like *b* remained unchanged as the reaction progressed. The globular morphology of the seeds is different from the elongated morphology of amyloid fibrils,[35] and to our knowledge radial expansion of fibrillar aggregates has not been previously described.

A number of seeds such as *a* sprouted fibrils as they grew, developed a coarse frayed periphery, and eventually lost their globular appearance. Other seeds showed a similar change to a coarser morphology but had no fibrils extending from them. The majority of seeds such as *b* stayed constant over the course of the reaction. The observation that some seeds became frayed as fibrils start to form, together with the distribution data in Figure 2 showing that smaller seeds predominate, suggests that large seeds are unstable and that the fibril morphology is preferred as the aggregation reaction progresses.

Fibril Elongation. Fibrils either extended from large seeds such as fibril *d* or grew in apparent isolation (*c*, *e*−*g*). On closer inspection, all fibrils can be traced back to small seeds or granules that have a larger fluorescence intensity than the fibrils that grow from them. In Figure 4, the granule starting points of the fibrils are indicated by lines pointing to their origin, whereas the ends of the growing fibrils are identified with arrows.

In previous TIRF studies with Aβ(1−40) and β2-microglobulin, fibril growth was observed to be unidirectional.[21,22] By contrast, previous AFM studies of amylin observed bidirectional growth of amylin fibrils, with elongation occurring from both ends.[36] We see apparent growth in multiple directions of the

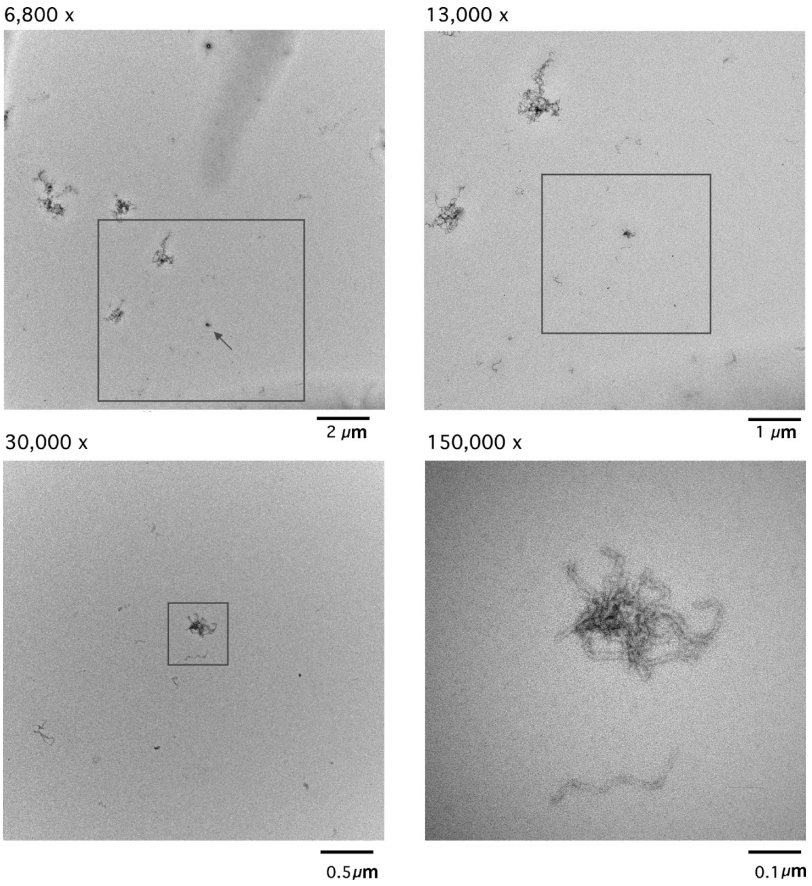

Figure 3. Electron micrographs of a granule-like seed (arrow) with a diameter of ~0.15 μm that at increasing magnification can be seen to be comprised of a cluster of fibrils. The EM data were recorded for a 100 μM amylin sample that was aggregated for 5 h at pH 8.

fibrils shown in Figure 4. For example fibril *e* slowly forms the top of the question-mark-shaped fibril between 870 and 1440 min. The bottom part of the question mark of fibril *e* then grows very rapidly after 1870 min. The top of fibril *f* grows toward seed *a* between 870 and 1870 min, but a fainter new arm of *f* extends in the opposite direction between 1320 and 2105 min. By contrast, fibril *g* grows in one direction, and fibril *c* is formed from the merging of the two branches *c* and *c*′ after 1155 min. After *c* and *c*′ have come together both the bottom-most arm and the arm on the left (*c*′) continue to grow in opposite directions, albeit at different rates. For all the fibrils that show apparent multidirectional growth (e.g., *c*, *e*, *f*) the elongation of the different branches is asynchronous with respect to the starting time and occurs at different rates. Moreover, all of the fibrils start to grow from a granule or small seed that appears as a nodule of higher fluorescence intensity than the fibrils that extends away from the origin (shown by the lines in Figure 4). For fibril *c*, *e*, and *f* the initial granules can be seen as early as 870 min. We think the data in Figure 4 are more consistent with multiple fibrils growing unidirectionally from a single seed. First, the extension of different arms occurs at different times during the reaction (for example, fibril *f*). Second, the elongation of different arms occurs with different rates. Third, growth in multiple directions in rosette-like bundles is observed from larger seeds such as *a*.

Fibril Thickening. The third process evident in the TIRFM data is an increase in the fluorescence intensity of some of the fibrils during the course of the reaction. We attribute this observation to growth of new fibrils along the templates provided by preformed fibrils, in a mechanism analogous to the "heterogeneous nucleation mechanism" first described for sickle cell hemoglobin fibrils.[29] Heterogeneous nucleation, also called "secondary nucleation", has been previously shown to play a role in amylin fibrillization based on kinetic studies.[30,31]

The intensity increases in preformed fibrils are best illustrated by fibril *d*, which is first observed in faint outline by 870 min (Figure 4). The fibril appears between two images collected in a 5 min interval and as such is likely to represent a fibril that has precipitated from solution.[21,22] Consequently, we have no information on the growth of fibril *d* before ~870 min. Once deposited on the slide, fibril *d* continues to grow slowly to close a lariat-like loop until 1870 min. In addition to these elongation processes, the fluorescence of fibril *d* becomes markedly more intense between 870 and 2895 min. The same type of increase in intensity is also seen for a number of the other fibrils including fibril *c* between 1195 and 2895 min. For reference, seed *b* maintains roughly the same intensity from the time it is first observed at 235 min to the end of the reaction at 2895 min, and fibril *g* shows little change in intensity between 1440 and 2895 min.

Fibrils are often observed in aligned bundles in high-resolution AFM and EM images. Since these structures are often wound around each other in a supercoil, it is unlikely they are formed by fibrils sticking together. One mechanism that could account for the growth of fibrils in bundles is the heterogeneous nucleation mechanism first proposed for sickle-cell hemoglobin fibrils.[29] Fibrils are first formed by homogeneous (or primary) nucleation

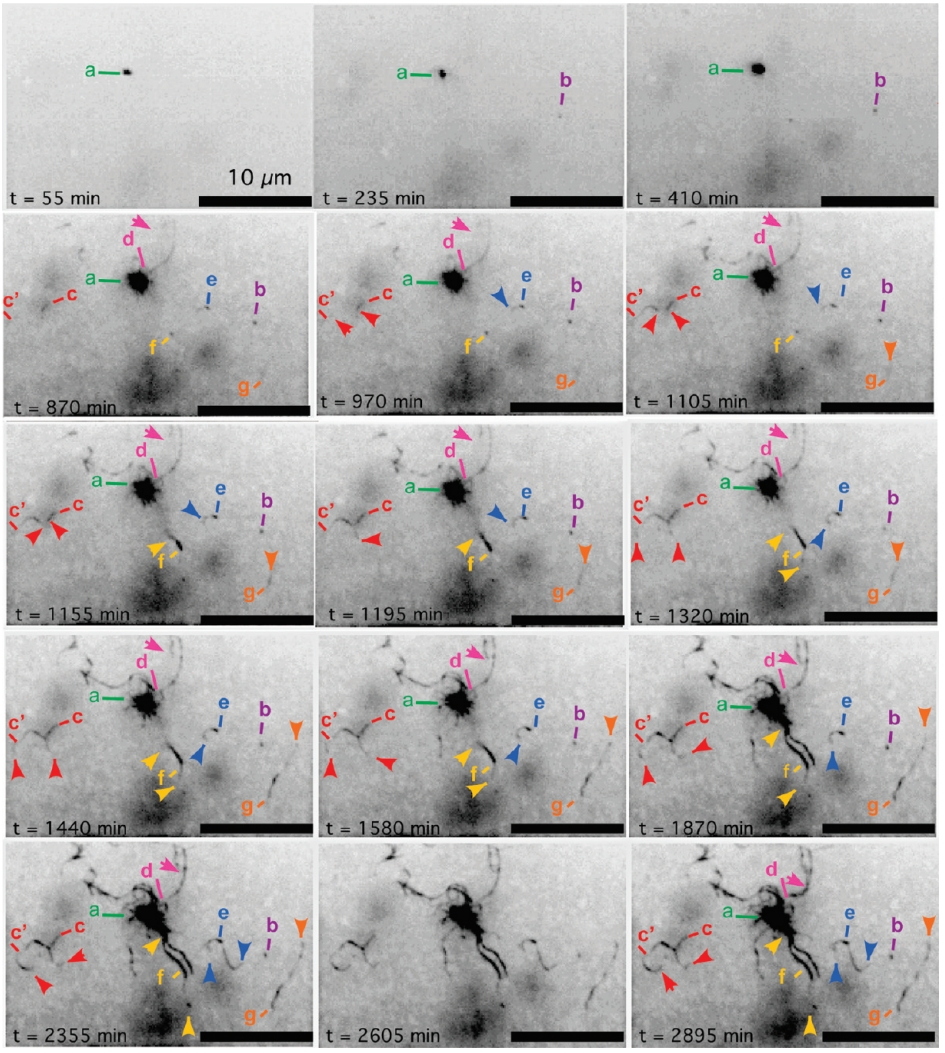

Figure 4. Snapshots of amylin fibril growth at pH 4 imaged by TIRFM. The time each image was obtained after transfer of dissolved amylin to a glass slide is given in the lower left-hand side of the panels. The data are from a total of 568 time points, recorded every 5 min for 2850 min (2 days). The time from preparing the sample to the first image collection was 45 min. Letters illustrate different species observed as described in the text. Lines are drawn to the location where each aggregate is seen at the earliest time point. Arrows indicate the ends of fibrils at the indicated time points.

during the lag time of the reaction and then elongate during the growth phase.[29,37] After an initial population of fibrils are formed, additional heterogeneous (or secondary) nucleation sites can became available along the length of preformed fibrils. These can promote the growth of new fibrils using the original fibrils as templates.[29] An alternative to this mechanism is that the strands in a bundle could grow simultaneously. Evidence for this mechanism was obtained from AFM imaging of amylin fibril growth on a mica surface.[33] On the basis of the TIRFM data, both types of mechanisms appear to have a role in amylin fibrillization. Fibril *f*, for example, is one of the most intensely fluorescent in Figure 4. The high fluorescence intensity of fibril *f* is maintained as it grows upward toward seed *a*, from 870 to 1870 min. An exception is in the frame at 1155 min, where a small thin, possibly frayed extension is seen for fibril *f* that grows in advance of the thicker fibril. To a good approximation, however, the growth of fibril *f* is consistent with a mechanism where if its stronger fluorescence intensity is due to a bundle rather than a single fibril, the strands in the bundle grow at the same time. In contrast to fibril *f*, the fibrils *c* and *d* start out as faint strands that increase in intensity with time, which is more readily explained by a template-assisted growth mechanism rather than simultaneous growth of strands in a bundle of fibrils. The increase in intensity of fibrils *c* and *d* is not distributed evenly throughout the fibril but appears to occur in patches or nodules that suggest the presence of multiple heterogeneous nucleation sites along the length of a fibril.

At the resolution of TIRFM we cannot accurately determine the width of fibrils.[21] Oscillation of fluorescence intensity could occur from fibrils diffusing in and out of the TIRFM illumination field. The changes we observe happen on time scales of hours (Figure 4), however, and we see increases in fluorescence intensity rather than the variations that would be expected if the fibrils were moving in and out of the evanescent field. Differential binding of ThT to the fibrils is another explanation that seems unlikely to account for the increase in fluorescence intensity since the initial staining of the fibrils occurs in less than 5 min. One possibility we cannot exclude is that preformed fibrils could be undergoing a conformational change that leads to increased ThT fluorescence. That the fluorescence increases

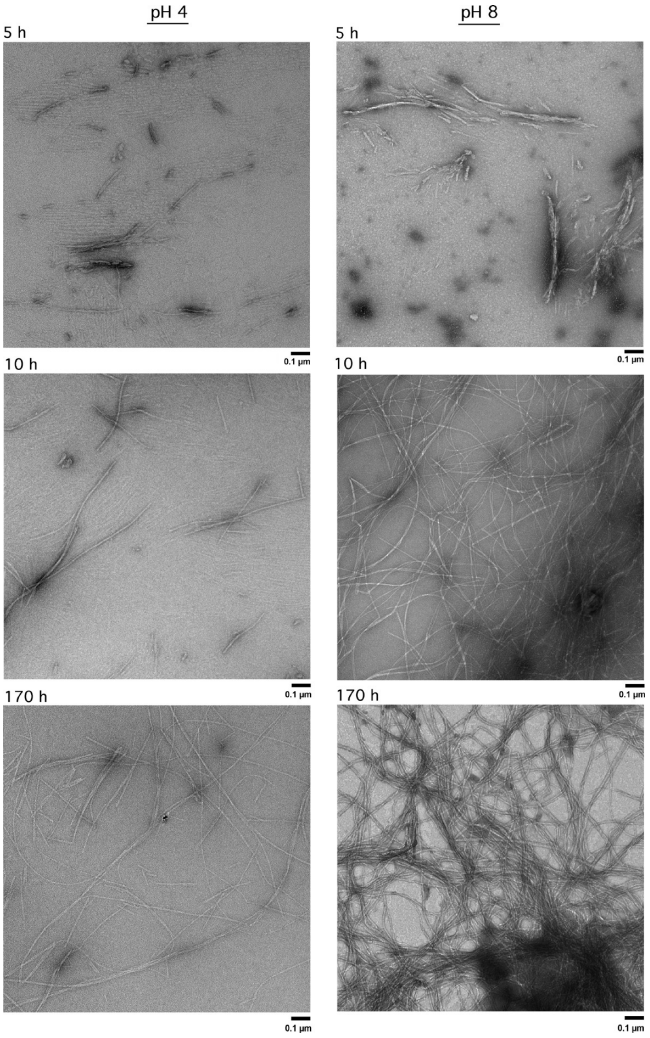

Figure 5. Time course of amylin fibrillization followed by EM. The panels on the left side show fibrils grown at pH 4 and the right side fibrils grown at pH 8. Images were sampled after solution incubation periods of 5 h (top), 10 h (middle), and 1 week (bottom). In contrast to the TIRFM (Figure 4), we cannot track the same aggregates over time by EM. To give a representative description, the images shown are the most typical of 5−10 images from different regions of the EM grid prepared for each time point and pH. All images are at a magnification of 68 000×.

occur progressively along the length of the fibrils and with rates similar to fibril growth seems more consistent with the formation of new fibrils than with changes in the properties of preformed fibrils.

Comparison of Fibril Growth by TIRFM and EM. In contrast to TIRFM where we can watch individual aggregates grow on the surface of a slide, EM can be used to image fibrils at high resolution after growth in bulk solution and transfer to a copper grid for uranyl acetate staining and imaging. We obtained EM images of amylin fibrils after aggregation times of 0.5, 5, 10, 20, and 170 h (1 week). For each time point we recorded five images from different areas of the grid and show the most representative for time points at 5, 10, and 170 h in Figure 5. Although EM is not suited for quantifying the amount of aggregates, we saw a qualitative increase in the number of fibrillar species with time, and more fibrils were formed at pH 8 than pH 4.

At the earliest time points in the reaction, between 0.5 and 5 h, the fibrils at pH 4 form sheets of very thin fibrils together with a smaller number of short robust fibrils (Figure 5). The fibrils formed during comparable times at pH 8 have a more frayed appearance (Figure 5). By 10 h, the sample at pH 4 shows a larger number of long fibrils together with the thin sheets of fibrils observed at earlier time points. In the pH 8 samples the fibrils formed by 10 h are longer and are more often arranged in curved coiled ribbon structures compared to the sticklike fibrils seen at pH 4. The last set of images in Figure 5 show the samples after 1 week (170 h), well after changes in TIRFM images had subsided (24−48 h). In the last time points, the fibrils at pH 8 reach lengths of 1−2 μm while at pH 4 some fibrils as short as 0.05−0.1 μm are still observed together with long fibrils (Figure 5). Note that these shorter fibrils at pH 4 would be too small to be resolved by TIRFM. The fibrils in the final time point at pH 8 are arranged in dense mesh works and have an average width of 14.4 ± 5.6 nm compared to 6.8 ± 1.9 at pH 4, consistent with previous reports that amylin fibrils at pH 8 are thicker than at pH 4.[28]

Kinetics of Individual Aggregate Growth. Figure 6 shows growth curves for seeds, fibrils, and the process we attribute to fibril thickening at pH 4 and 8. Kinetic parameters obtained from least-squares fits of the data are summarized in Table 1. Under both conditions seed growth is observed first followed by fibril elongation and fibril thickening. Because many of the seeds we looked at were already present at the start of the reaction, we consider the lag time for seed formation undefined in the TIRFM experiment. On the basis of solution experiments, the lag times for fibrillization under the conditions of the TIRFM experiments (samples in 10% acetonitrile) are about 30 min (Figure 7, Table 1), which is shorter than the ∼45 min dead time of the TIRFM experiments. The apparent average lag time for species with a distinct fibrillar morphology by TIRFM is much longer: about 4 h at pH 8 (Figure 6B) and 14 h at pH 4 (Figure 6D). We note that in the earliest stages of the TIRFM experiments most of the ThT fluorescence is due to seeds, which are likely to be composed of plaques or clusters of fibrils too small to resolved by TIRFM. Fibril thickening had the longest lag times between 26 and 37 h at pH 4 and between 3 and 4 h at pH 8 (Figure 6C,F). Radial seed growth had the slowest rate, fibril elongation rates were intermediate, and fibril thickening rates were the fastest (Table 1). Comparing the reactions at the two pH values, all processes had longer lag times and slower growth rates at pH 4 compared to pH 8 (Table 1).

At the completion of the reactions we could measure the maximum dimensions of the individual aggregates used to characterize fibrillization kinetics by TIRFM. The averages of these values are given in Table 1. We saw no correlation between growth rates and the final sizes of individual seeds or fibrils. The final dimensions for the thickening process are shorter than for elongation because the increases in fluorescence intensity often occurs in patches along the length of a fibril, and we only characterized the growth kinetics of uninterrupted segments.

Fibrillization Kinetics in Solution. Figure 7 shows kinetic data for amylin fibrillization in solution. The reactions were carried out at the same 100 μM amylin concentration and 25 °C temperature as the TIRFM experiments. For one set of experiments monomeric amylin was initially dissolved in ACN and brought up in buffer to a final concentration 10% ACN (v/v). This set of conditions is the same as for the TIRFM and EM experiments shown in Figures 1−6. We also looked at amylin that was initially dissolved in DMSO[28] and brought up in buffer to a final concentration of 4% DMSO (v/v). The first 10 h of the reactions shows a sigmoidal profile typical of a nucleated

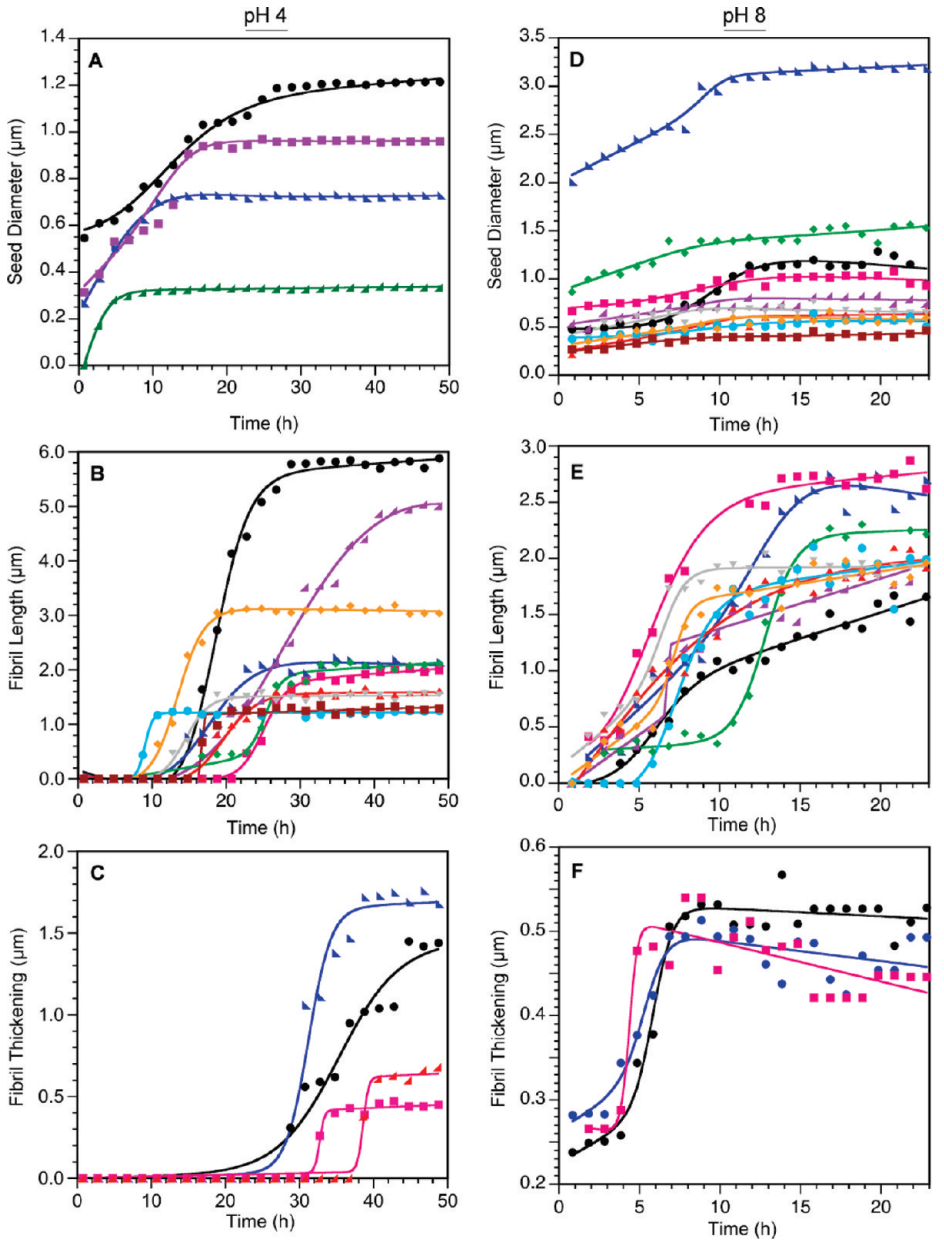

Figure 6. Kinetics of individual seed growth, fibril elongation, and fibril thickening from TIRFM data at pH 4 (A, B, C) and pH 8 (D, E, F). The data for each fibril were fitted to a six-parameter equation[38] in order to extract lag times, growth rates, and maximal length parameters, which are given in Table 1.

fibrillization reaction consisting of a lag time, a growth phase, and a plateau.[37,38] This portion of the data were fitted to a six-parameter model[38] to obtain the kinetic parameters for the solution reactions given in Table 1. The lag times obtained in solution are much shorter than the lag times for fibril growth obtained for the fibrils imaged by TIRFM. The rates of fibril growth are slower for individual fibrils but within a factor of 2 of the solution rates (Table 1). Part of the reason for this difference is that in the TIRFM experiment we are measuring the kinetics of the longest fibrils in the reaction (1−8 μm), whereas the majority of the fibrils formed in the early stages of the reaction are too short to be discerned as such at the resolution of the TIRF microscope (<0.5 μm). When considering differences in elongation rates between the experiments, it is also important to note that in solution we are measuring only ThT fluorescence, which does not distinguish between the species with different morphologies or different growth processes observed by TIRFM.

At time points following the initial leveling off of fluorescence after 10 h, the solution reactions show behavior that deviates from standard fibrillization time curves. In 4% DMSO solvent, there is a decrease in fluorescence following the initial plateau. It has been argued that once fibrils have formed the solution is no longer homogeneous so that fluorescence measurements become erratic and are of questionable value.[39] At amylin concentrations below 20 μM the plateaus in 4% DMSO are nearly flat, suggesting that the decreasing plateau at 100 μM amylin may be due to an increase in the turbidity of the samples accompanying the formation of insoluble fibrils. For the 10% ACN solvent, we see a reproducible increase in fluorescence following the initial fluorescence plateau. This increase in fluorescence following an

dx.doi.org/10.1021/bi101908m |*Biochemistry* 2011, 50, 2808–2819

Table 1. Growth Rates of ThT-Sensitive Amylin Aggregates[a]

conditions	lag time (h)	growth rate (μm/h)	max length (μm)	species averaged
pH 4				
seed diameter	N.D.[e]	0.27 ± 0.04	0.81 ± 0.18	4
fibril elongation	14.14 ± 1.54	0.56 ± 0.09	2.60 ± 0.51	10
fibril thickening	31.3 ± 2.4	1.75 ± 0.76	1.08 ± 0.31	4
solution (10% ACN, pt 1)[b,c]	0.59 ± 0.35	1.20 ± 0.02	N.A.[f]	N.A.[f]
solution (10% ACN, pt 2)[b,d]	11.93 ± 2.09	0.74 ± 0.25	N.A.[f]	N.A.[f]
solution (4% DMSO)[b]	2.56 ± 0.34	1.70 ± 0.30	N.A.[f]	N.A.[f]
pH 8				
seed diameter	N.D.[e]	0.70 ± 0.09	1.06 ± 0.26	10
fibril elongation	4.31 ± 1.11	0.73 ± 0.18	2.10 ± 0.13	9
fibril thickening	4.18 ± 0.25	2.35 ± 0.83	0.48 ± 0.02	3
solution (10% ACN)[b]	0.42 ± 0.01	1.15 ± 0.01	N.A.[f]	N.A.[f]
solution (4% DMSO)[b]	0.04 ± 0.04	1.32 ± 0.01	N.A.[f]	N.A.[f]

[a] Rates for the different growth processes were obtained by nonlinear least-squares fits of the kinetic curves in Figures 6 and 7 as described.[38] Rate constants are reported as means ±1 standard error. Note that the uncertainties for the TIRF data describe the variation between individual aggregates (Figure 6) while for the solution data (Figure 7) they were obtained from duplicate measurements of solution population-weighted averages. [b] The units for the fibril growth rates from solution experiments are fluorescence intensity (arbitrary units)/h. For solution experiments, except 10% ACN at pH 4, kinetic parameters were calculated by considering only the first 10 h of the reactions which show a sigmoidal time dependence characteristic of fibrillization. [c] Kinetic parameters derived from the first part of the reaction between 0 and 10 h. [d] Kinetic parameters derived from the second part of the reaction between 8 and 30 h. [e] Not determined since many of the seeds are already visible in the first images recorded at both pH 4 and pH 8. The dead time for the TIRF experiments was ~45 min. [f] Not applicable.

initial steady state is observed for fibrillization reactions where the amylin concentration is as low as 5 μM and suggests that fibrils continue to form after the first 10 h of the reaction. At pH 4 this is manifested as a second sigmoidal curve that starts after the first apparent plateau is reached (Figure 7A). Note that the increase in florescence intensity during the second sigmoidal phase is about 40% of the increase in the first sigmoidal phase that occurs within the first 10 h of the reaction. At pH 8 we also see a continuing increase in fluorescence after the initial sigmoidal phase, with a shallower apparently linear time dependence that does not subside by 30 h (Figure 7B). In this case as well, the increase in fluorescence between 10 and 30 h is about 70% of the increase in fluorescence during the first 10 h of the reaction. The increases in ThT fluorescence during the second stage of the reaction suggests that fibrils are formed through secondary nucleation, catalyzed by the initial population of fibrils that grew during the first 10 h.

If we compare the time course of the individual aggregates measured by TIRFM to the solution data, the largest seeds that we could measure accurately at pH 4 formed between 0 and 20 h (Figure 6A), a time that extends beyond the first 10 h sigmoidal phase of the solution reaction in 10% ACN (Figure 7A). Fibrils grew between 9 and 40 h (Figure 6B)—a time that also extends past the first and into the second sigmoidal phase of the reaction in solution (Figure 7A). Consequently, the lag times and elongation rates of the fibrils observed by TIRFM are in much better agreement with the kinetic parameters obtained from the second phase of the solution reaction (Table 1). The increases in fluorescence intensities of the fibrils imaged by TIRFM occur between 20 and 40 h (Figures 4 and 5C), well past the first 10 h sigmoidal phase of the solution reaction (Figure 7A). Finally, the changes in fibril morphology and association by EM (Figure 5) occur on slower time scales than the first 10 h transition seen for the solution reaction at pH 4 with 10% ACN (Figure 7A). At pH 8 where fibrillization is faster, the growth of individual seeds (Figure 6C) and fibrils (Figure 6D) is more comparable to the solution rates (Figure 7B), but asynchronicity is still observed, with some individual fibrils imaged by TIRFM growing after the first fluorescence plateaus is reached in bulk solution.

In the presence of 4% DMSO the rate of fibrillization is increased and the reactions reach a larger ThT fluorescence plateau, suggesting that more fibrils are formed than with 10% ACN (Figure 7). We found that increasing the DMSO concentration between 1% and 10% (v/v) promotes fibrillization primarily by increasing the elongation rate of the reaction (Supporting Information). Thus, DMSO appears to act as a catalyst for fibrillization. By contrast, at large concentrations (≥95%) DMSO disaggregates fibrils to monomers [Alexandrescu, A. T., unpublished observations]. Given the differences in solution reaction profiles between samples dissolved in 10% ACN and 4% DMSO, we collected additional TIRFM data to examine the time dependence of fibrillization of a 100 μM amylin sample at pH 8 in 4% DMSO (Supporting Information). Compared to samples in 10% ACN, the sample in 4% DMSO fibrillized much faster and the appearance of fibrils was more abrupt, resembling a phase transition. Most fibrils formed in 2 h in the TIRFM experiment—a time more in line with the reaction in solution (Figure 7B). We saw examples of all three growth mechanisms observed with 10% ACN: seed growth, fibril elongation, and fibril thickening. Of the three, however, fibril growth appeared to be the more dominant process with 4% DMSO. These observations suggest primary nucleation is favored over secondary nucleation in 4% DMSO compared to 10% ACN. It is interesting to note in this regard that organic phases such as dichloromethane, chloroform, or lipid bilayers have been shown to accelerate the fibrillization of a 20−29 fragment of amylin and to shift the balance from secondary to primary fibril nucleation mechanisms.[31]

DISCUSSION

TIRFM shows three types of amylin fibrillization processes: seed growth, elongation, and fibril thickening. Seeds are the earliest species seen and are likely to consist of plaques of short fibrils

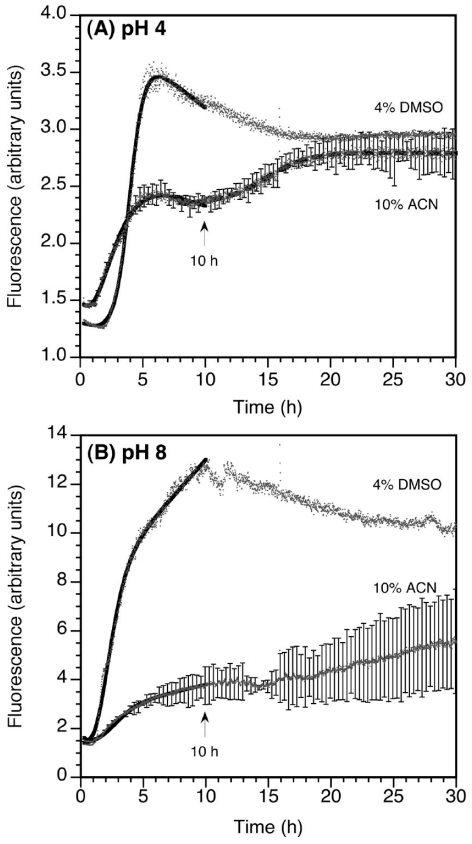

Figure 7. Kinetics of fibrillization in solution followed by ThT fluorescence at pH 4 (A) or pH 8 (B). For each pH, samples were initially dissolved in ACN and brought up in buffer to a final concentration of 10% (v/v) ACN or in DMSO and brought up to a final concentration of 4% (v/v) DMSO. The data for each set of conditions are averages of duplicate measurements. Representative errors are shown for 5% of the data points in the ACN experiments, and errors in kinetic parameters from the duplicate data sets are given in Table 1. The data for the first 10 h only were fitted to a six-parameter equation[38] to obtain values for lag times and rate constants which are given in Table 1. For the pH 4 data in the presence of 10% ACN we separately fitted the data between 8 and 30 h to a second sigmoidal transition (dashed curve). For the other experiments the data beyond 10 h do not define a sigmoidal transition and were not fit.

based on their size, growth rates, and ThT binding. Fibrils invariably elongate from small seeds or granules, except for some rare cases where we see fibrils apparently branch from other fibrils (Supporting Information) in a mechanism similar to that observed in TIRFM studies of glucagon fibrillization.[20] Fibril elongation appears to be unidirectional, if we consider that multiple fibrils can grow in opposite directions with different rates, starting from a common seed. A third type of process is manifested as a progressive increase in the fluorescence intensity of preformed fibrils. We attribute the fluorescence intensity increases to template-assisted growth of fibrils alongside preformed fibrils. The fluorescence intensity increases often occur in patches, suggesting that multiple secondary nucleation sites can occur along the length of a fibril. We also see instances of fibrils that grow with a uniformly high fluorescence intensity from start to finish (upper branch of fibril *f* in Figure 4), which could be consistent with the simultaneous growth of strands in a bundle of fibrils as has previously seen in AFM experiments.[33]

Although the three types of aggregation processes (seed growth, fibril elongation, and fibril thickening) manifest themselves differently by TIRFM, they may occur by the same mechanism, namely heterogeneous or secondary nucleation. This seems consistent with the time course of the growth processes imaged by TIRFM and EM, which for samples in 10% ACN occur after the completion of the main phase of the reaction in bulk solution. In the classical nucleation mechanism, aggregation is initially disfavored by entropy since association involves loss of rotational and translational degrees of freedom for the monomers. The time required to form the "critical nuclei" that propagate polymerization is manifested as a lag time, during which aggregation is not detected.[29] Once critical nuclei are formed in a process called "homogeneous" or "primary" nucleation, the reaction enters a growth phase as the loss of entropy for the monomers is compensated by the gain in enthalpy due to the formation of new noncovalent interactions when the monomers become incorporated into the growing fibril.[29] The reaction proceeds, reaching an eventual plateau that depends on the solubility of the monomers. In a double nucleation mechanism, fibrils can form through homogeneous or primary nucleation steps but can also be initiated by heterogeneous or secondary nucleation on the surfaces of preformed fibrils.[29,40] Additional mechanisms that could play a role in secondary nucleation include branching of fibrils or fragmentation of fibrils in a way that introduces new sites for incorporation of monomers.[31] Elegant studies by the Miranker lab, looking at the dependence of polymerization kinetics on monomer and seed concentrations, established that secondary nucleation is the predominant mechanism of amylin fibrillization in aqueous solution.[30,31] Additional amyloidogenic proteins for which secondary nucleation appears to play a role in fibrillization include Aβ,[41] prion protein,[42] β2-microglobulin,[43] insulin,[44] and glucagon.[20]

Secondary nucleation may be significant in the progression of amyloid diseases. In the case of type 2 diabetes, once a population of amylin fibrils is established it could facilitate the formation of new fibrils through secondary nucleation, as fresh hormone is released from the pancreatic β-cells into the extracellular matrix. One strategy to inhibit fibrillogenesis is to develop compounds that interfere with the formation of the primary nuclei needed for fibril formation. However, if primary and secondary nucleation have a different structural basis, interfering with primary nucleation may not be effective in controlling secondary nucleation once a population of fibrils has been established.

■ ASSOCIATED CONTENT

Supporting Information. Movies of fibrillization reactions, dependence of solution fibrillization rates on DMSO and ACN concentrations, TIRFM data for fibrils grown in the presence of 4% DMSO, TIRFM images of fibrils grown in bulk solution and additional figures. This material is available free of charge via the Internet at http://pubs.acs.org.

■ AUTHOR INFORMATION

Corresponding Author

*Tel: (860) 486-4414. Fax: (860) 486-4331. E-mail: andrei@uconn.edu.

Funding Sources

This work was funded by Basic Science Award 1-10-BS-04 from the American Diabetes Association.

■ ACKNOWLEDGMENT

We thank Prof. David Knecht, Dr. Carol Norris, and Sarah Sheftic for useful discussions.

■ ABBREVIATIONS

ACN, acetonitrile; AFM, atomic force microscopy; DMSO, dimethyl sulfoxide; EM, electron microscopy; IAPP, islet amyloid polypeptide; ThT, thioflavin T; TIRFM, total internal reflection fluorescence microscopy.

■ REFERENCES

(1) Clark, A., Cooper, G. J., Lewis, C. E., Morris, J. F., Willis, A. C., Reid, K. B., and Turner, R. C. (1987) Islet amyloid formed from diabetes-associated peptide may be pathogenic in type-2 diabetes. *Lancet 2*, 231–234.

(2) Clark, A., and Nilsson, M. R. (2004) Islet amyloid: a complication of islet dysfunction or an aetiological factor in Type 2 diabetes?. *Diabetologia 47*, 157–169.

(3) Cooper, G. J. (1994) Amylin compared with calcitonin gene-related peptide: structure, biology, and relevance to metabolic disease. *Endocr. Rev. 15*, 163–201.

(4) Gotz, J., Ittner, L. M., and Lim, Y. A. (2009) Common features between diabetes mellitus and Alzheimer's disease. *Cell. Mol. Life Sci. 66*, 1321–1325.

(5) Zdrojewicz, Z., and Belowska-Bién, K. (2006) Amylin - structure, function, clinical meaning. *Diabetol. Dosw. Klin. 6*, 169–172.

(6) Janson, J., Ashley, R. H., Harrison, D., McIntyre, S., and Butler, P. C. (1999) The mechanism of islet amyloid polypeptide toxicity is membrane disruption by intermediate-sized toxic amyloid particles. *Diabetes 48*, 491–498.

(7) Lorenzo, A., Razzaboni, B., Weir, G. C., and Yankner, B. A. (1994) Pancreatic islet cell toxicity of amylin associated with type-2 diabetes mellitus. *Nature 368*, 756–760.

(8) Matveyenko, A. V., and Butler, P. C. (2006) Islet amyloid polypeptide (IAPP) transgenic rodents as models for type 2 diabetes. *ILAR J. 47*, 225–233.

(9) Anguiano, M., Nowak, R. J., and Lansbury, P. T., Jr. (2002) Protofibrillar islet amyloid polypeptide permeabilizes synthetic vesicles by a pore-like mechanism that may be relevant to type II diabetes. *Biochemistry 41*, 11338–11343.

(10) Engel, M. F. (2009) Membrane permeabilization by Islet Amyloid Polypeptide. *Chem. Phys. Lipids 160*, 1–10.

(11) Haataja, L., Gurlo, T., Huang, C. J., and Butler, P. C. (2008) Islet amyloid in type 2 diabetes, and the toxic oligomer hypothesis. *Endocr. Rev. 29*, 303–316.

(12) Meng, F., Marek, P., Potter, K. J., Verchere, C. B., and Raleigh, D. P. (2008) Rifampicin does not prevent amyloid fibril formation by human islet amyloid polypeptide but does inhibit fibril thioflavin-T interactions: implications for mechanistic studies of beta-cell death. *Biochemistry 47*, 6016–6024.

(13) Sakagashira, S., Sanke, T., Hanabusa, T., Shimomura, H., Ohagi, S., Kumagaye, K. Y., Nakajima, K., and Nanjo, K. (1996) Missense mutation of amylin gene (S20G) in Japanese NIDDM patients. *Diabetes 45*, 1279–1281.

(14) Ma, Z., Westermark, G. T., Sakagashira, S., Sanke, T., Gustavsson, A., Sakamoto, H., Engstrom, U., Nanjo, K., and Westermark, P. (2001) Enhanced in vitro production of amyloid-like fibrils from mutant (S20G) islet amyloid polypeptide. *Amyloid 8*, 242–249.

(15) Amos, A. F., McCarty, D. J., and Zimmet, P. (1997) The rising global burden of diabetes and its complications: estimates and projections to the year 2010. *Diabet. Med. 14* (Suppl 5), S1–85.

(16) Hogan, P., Dall, T., and Nikolov, P. (2003) Economic costs of diabetes in the US in 2002. *Diabetes Care 26*, 917–932.

(17) Ban, T., and Goto, Y. (2006) Direct observation of amyloid growth monitored by total internal reflection fluorescence microscopy. *Methods Enzymol. 413*, 91–102.

(18) Fish, K. N. (2009) Total internal reflection fluorescence (TIRF) microscopy, *Curr. Protoc. Cytom. Chapter 12*, Unit12 18.

(19) Schneckenburger, H. (2005) Total internal reflection fluorescence microscopy: technical innovations and novel applications. *Curr. Opin. Biotechnol. 16*, 13–18.

(20) Andersen, C. B., Yagi, H., Manno, M., Martorana, V., Ban, T., Christiansen, G., Otzen, D. E., Goto, Y., and Rischel, C. (2009) Branching in amyloid fibril growth. *Biophys. J. 96*, 1529–1536.

(21) Ban, T., Hamada, D., Hasegawa, K., Naiki, H., and Goto, Y. (2003) Direct observation of amyloid fibril growth monitored by thioflavin T fluorescence. *J. Biol. Chem. 278*, 16462–16465.

(22) Ban, T., Hoshino, M., Takahashi, S., Hamada, D., Hasegawa, K., Naiki, H., and Goto, Y. (2004) Direct observation of Abeta amyloid fibril growth and inhibition. *J. Mol. Biol. 344*, 757–767.

(23) Ozawa, D., Yagi, H., Ban, T., Kameda, A., Kawakami, T., Naiki, H., and Goto, Y. (2009) Destruction of amyloid fibrils of a beta2-microglobulin fragment by laser beam irradiation. *J. Biol. Chem. 284*, 1009–1017.

(24) LeVine, H., 3rd. (1993) Thioflavine T interaction with synthetic Alzheimer's disease beta-amyloid peptides: detection of amyloid aggregation in solution. *Protein Sci. 2*, 404–410.

(25) Collins, S. R., Douglass, A., Vale, R. D., and Weissman, J. S. (2004) Mechanism of prion propagation: amyloid growth occurs by monomer addition. *PLoS Biol. 2*, e321.

(26) Inoue, Y., Kishimoto, A., Hirao, J., Yoshida, M., and Taguchi, H. (2001) Strong growth polarity of yeast prion fiber revealed by single fiber imaging. *J. Biol. Chem. 276*, 35227–35230.

(27) Liang, Y., Lynn, D. G., and Berland, K. M. (2010) Direct observation of nucleation and growth in amyloid self-assembly. *J. Am. Chem. Soc. 132*, 6306–6308.

(28) Abedini, A., and Raleigh, D. P. (2005) The role of His-18 in amyloid formation by human islet amyloid polypeptide. *Biochemistry 44*, 16284–16291.

(29) Ferrone, F. A., Hofrichter, J., and Eaton, W. A. (1985) Kinetics of sickle hemoglobin polymerization. II. A double nucleation mechanism. *J. Mol. Biol. 183*, 611–631.

(30) Padrick, S. B., and Miranker, A. D. (2002) Islet amyloid: phase partitioning and secondary nucleation are central to the mechanism of fibrillogenesis. *Biochemistry 41*, 4694–4703.

(31) Ruschak, A. M., and Miranker, A. D. (2007) Fiber-dependent amyloid formation as catalysis of an existing reaction pathway. *Proc. Natl. Acad. Sci. U.S.A. 104*, 12341–12346.

(32) Abramoff, M. D., Magelhaes, P. J., and Ram, S. J. (2004) Image processing with ImageJ. *Biophoton. Int. 11*, 36–42.

(33) Green, J. D., Goldsbury, C., Kistler, J., Cooper, G. J., and Aebi, U. (2004) Human amylin oligomer growth and fibril elongation define two distinct phases in amyloid formation. *J. Biol. Chem. 279*, 12206–12212.

(34) Wu, J. W., Breydo, L., Isas, J. M., Lee, J., Kuznetsov, Y. G., Langen, R., and Glabe, C. (2010) Fibrillar oligomers nucleate the oligomerization of monomeric amyloid beta but do not seed fibril formation. *J. Biol. Chem. 285*, 6071–6079.

(35) Dobson, C. M. (2003) Protein folding and misfolding. *Nature 426*, 884–890.

(36) Goldsbury, C., Kistler, J., Aebi, U., Arvinte, T., and Cooper, G. J. (1999) Watching amyloid fibrils grow by time-lapse atomic force microscopy. *J. Mol. Biol. 285*, 33–39.

(37) Harper, J. D., and Lansbury, P. T., Jr. (1997) Models of amyloid seeding in Alzheimer's disease and scrapie: mechanistic truths and physiological consequences of the time-dependent solubility of amyloid proteins. *Annu. Rev. Biochem. 66*, 385–407.

(38) Cohlberg, J. A., Li, J., Uversky, V. N., and Fink, A. L. (2002) Heparin and other glycosaminoglycans stimulate the formation of amyloid fibrils from alpha-synuclein in vitro. *Biochemistry 41*, 1502–1511.

(39) Volles, M. J., and Lansbury, P. T., Jr. (2007) Relationships between the sequence of alpha-synuclein and its membrane affinity, fibrillization propensity, and yeast toxicity. *J. Mol. Biol. 366*, 1510–1522.

(40) Ferrone, F. A., Ivanova, M., and Jasuja, R. (2002) Heterogeneous nucleation and crowding in sickle hemoglobin: an analytic approach. *Biophys. J. 82*, 399–406.

(41) Hortschansky, P., Schroeckh, V., Christopeit, T., Zandomeneghi, G., and Fandrich, M. (2005) The aggregation kinetics of Alzheimer's beta-amyloid peptide is controlled by stochastic nucleation. *Protein Sci. 14*, 1753–1759.

(42) Knowles, T. P., Waudby, C. A., Devlin, G. L., Cohen, S. I., Aguzzi, A., Vendruscolo, M., Terentjev, E. M., Welland, M. E., and Dobson, C. M. (2009) An analytical solution to the kinetics of breakable filament assembly. *Science 326*, 1533–1537.

(43) Xue, W. F., Homans, S. W., and Radford, S. E. (2008) Systematic analysis of nucleation-dependent polymerization reveals new insights into the mechanism of amyloid self-assembly. *Proc. Natl. Acad. Sci. U.S.A. 105*, 8926–8931.

(44) Fodera, V., Cataldo, S., Librizzi, F., Pignataro, B., Spiccia, P., and Leone, M. (2009) Self-organization pathways and spatial heterogeneity in insulin amyloid fibril formation. *J. Phys. Chem. B 113*, 10830–10837.